

Review

Large Eddy Simulation of Flow and Heat Transfer in a Ribbed Channel for the Internal Cooling Passage of a Gas Turbine Blade: A Review

Joon Ahn 

School of Mechanical Engineering, Kookmin University, 77 Jeongneung-ro, Seongbuk-gu, Seoul 02707, Republic of Korea; jahn@kookmin.ac.kr

Abstract: Herein, 50 articles published over the past 20 years on using large eddy simulation (LES) for the internal cooling passage of a gas turbine, especially the mid-chord ribbed channel, are reviewed for the first time. First, the numerical challenges of performing LES on a ribbed channel and experimental verification are summarized. Next, LES data and the major engineering findings that are difficult to obtain experimentally or using Reynolds-averaged Navier–Stokes simulation (RANS) are covered, and heat transfer on and inside the rib, and the effects of rotation and buoyancy are discussed. Next, recent LES studies related to the shape of the ribbed channel are reviewed, and finally, the contribution of using LES for research on the internal cooling of gas turbines in the future, including those with ribbed channels, is anticipated.

Keywords: large eddy simulation (LES); local heat transfer; conjugate heat transfer; rotation; rib geometry



Citation: Ahn, J. Large Eddy Simulation of Flow and Heat Transfer in a Ribbed Channel for the Internal Cooling Passage of a Gas Turbine Blade: A Review. *Energies* **2023**, *16*, 3656. <https://doi.org/10.3390/en16093656>

Academic Editor: Artur Bartosik

Received: 6 March 2023

Revised: 21 April 2023

Accepted: 21 April 2023

Published: 24 April 2023



Copyright: © 2023 by the author. Licensee MDPI, Basel, Switzerland. This article is an open access article distributed under the terms and conditions of the Creative Commons Attribution (CC BY) license (<https://creativecommons.org/licenses/by/4.0/>).

1. Introduction

Gas turbines are widely used for land-based power generation as well as aircraft and ship propulsion due to their large power-to-weight ratio. Increasing the turbine inlet total temperature (TITT) and compression ratio can improve the cycling efficiency and power output of gas turbines [1]. Advancements in turbine cooling have enabled engine design to exceed the temperature limitation of the commonly used materials [2]. As shown in Figure 1a, a turbine is cooled by extracting some of the compressor air while maximizing the cooling effect with the minimum amount of air [3].

As shown in Figure 1a, the coolant is supplied to the blade to cool the inside and then discharged through a hole in the surface to form an insulating film. As shown in Figure 1b, the cooling channel consists of multiple passes, and components that promote heat transfer are applied to each part. In most regions, ribs are installed as heat transfer promoters. An impinging jet is applied to the leading edge, and a pin fin or dimple is sometimes installed on the trailing edge where it is difficult to install a rib [4,5].

Recently, studies on heat transfer in a triangular channel simulating a trailing edge or pin fin have been conducted [6], and research on heat transfer in an impinging jet or a semicircular channel at a leading edge has also been published [7]. However, most of the middle portion can be seen as a ribbed channel [8], which is the most commonly studied among the gas turbine internal cooling methods [9].

The cooling passage of a gas turbine blade can be modeled as a ribbed channel (Figure 2a) [10]. The ribs promote heat transfer while separating/reattaching the flow in the passage (Figure 2b) [11,12]. Since the heat transfer augmentation effect of the ribs decreases as the heat flows downstream, several of them are installed periodically. To enhance the heat transfer effect, the downstream rib must be located after the reattachment point, so the installation period (p) is usually around 10 times the height of the rib (e) [13].

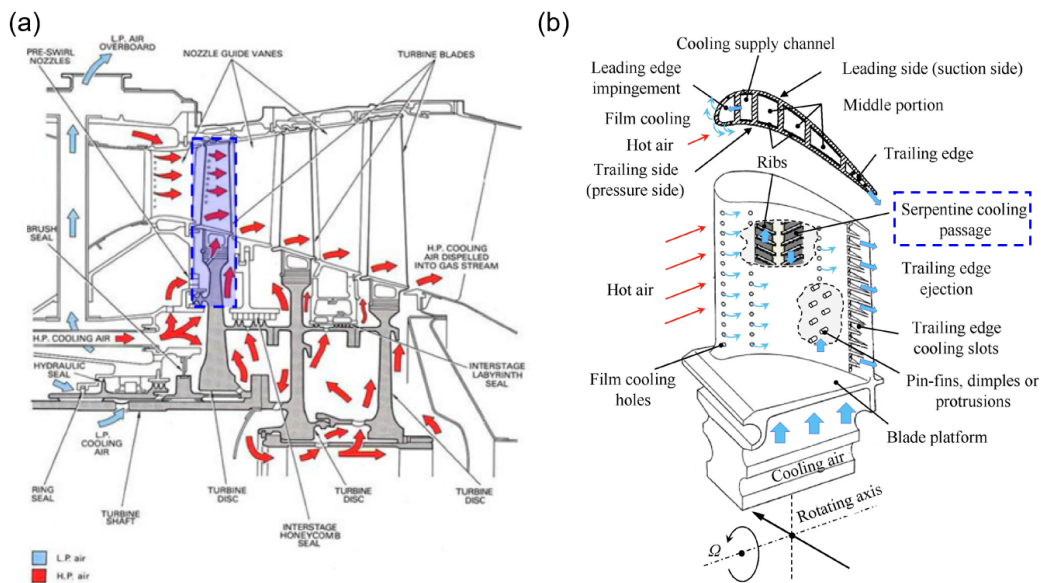


Figure 1. Cooling of gas turbine blades: (a) The air supply system for gas turbine cooling [3]; (b) gas turbine blades with cooling applied [4].

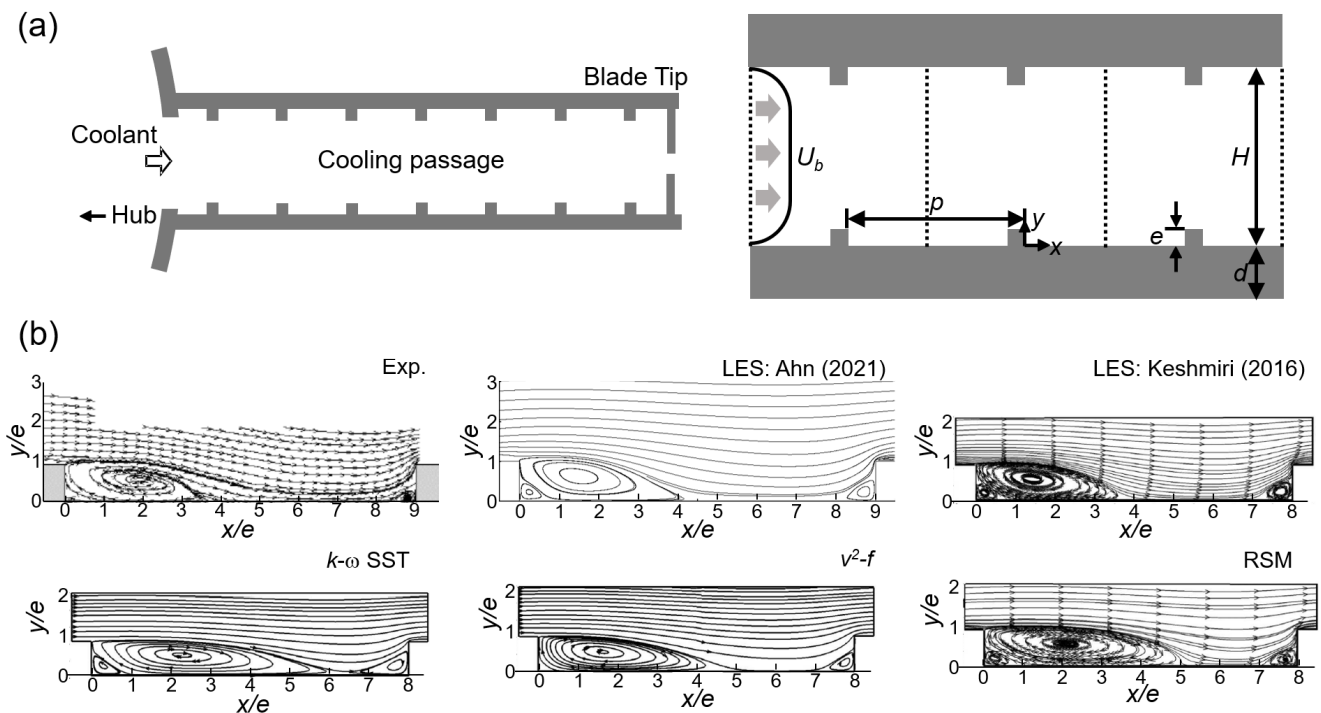


Figure 2. Modeling and flow patterns of gas turbine internal cooling passages: (a) the ribbed channel modeling cooling passage [11]; (b) streamlines in ribbed channels obtained experimentally [11] and using computational fluid dynamics (CFD) [10,12]. LES: large eddy simulation; p : installation period; e : rib height; U_b : bulk velocity; H : channel height; d : wall thickness; x : streamwise coordinate; y : wall-normal coordinate; SST: shear stress transport model; v^2 , the velocity fluctuation normal to the streamlines; f : an elliptic relaxation function; RSM: Reynolds stress model.

As shown in Figure 2b, there is a recirculation area behind the rib where heat transfer is poor, and rib turbulators with various geometries were developed to improve this [14]. Measurement techniques such as thermochromic liquid crystal (TLC) [15] or infrared cameras [16] are applied to obtain the local heat transfer distribution. When applying these

techniques to the experimental setup to consider the rotation effect, it is sometimes difficult to rotate the optical equipment such as a camera along with the test section [17].

The rib also serves as a fin that expands the heat exchange area, while promoting heat transfer in the experimentally obtained channel heat transfer data on ribs is very rare because it is difficult to impose boundary conditions on them while gaining optical access from the front and back sides of the ribs [18]. By performing computational fluid dynamics (CFDs) simulation, the heat transfer distribution of the rib can be obtained and the effect of rotation, which is also difficult to deal with experimentally, can also be observed [19].

The Reynolds-averaged Navier–Stokes simulation (RANS) technique depending on a semi-empirical model is most often used to analyze the fluid flow and heat transfer in the gas turbine blades' cooling channel [19]. However, a variation of around 250% was found between different RANS models when predicting ribbed channel flow heat transfer [20]. In recent years, large eddy simulation (LES) has been used to study the internal cooling of turbine blades as it reduces the uncertainty of heat transfer prediction using RANS to within 1/4 [21].

Research on ribbed channels applied to gas turbine cooling passages began in the 1970s, with the first review papers being published in this recently [22], mostly including experimental results [7,17]. In the most recent reviews of CFD data on heat transfer in ribbed channels [23], the target was a solar heater rather than a gas turbine blade, and thus analysis of the rotation effect, etc., was not included and only RANS results were reported. CFD studies on the ribbed channel of a gas turbine blade were reviewed in 1995 [24], which is before using LES started in earnest.

The first articles on using LES to analyze gas turbine cooling passages were published in the early 2000s [25], with over 50 appearing over the past 20 years. LES can be used to predict the heat transfer mechanism more closely to the experimental findings than RANS, and provides information that is difficult to obtain experimentally, such as on instantaneous temperature fields and turbulent heat transfer. The internal cooling passage problem in a gas turbine includes the heat transfer mechanism that is difficult to predict using RANS. Since there are relatively few difficulties in the numerical analysis using LES, we anticipate that it will become more widely used in the industry in the future [20,21].

The LES results for ribbed channels from 50 articles are summarized in Table 1. In this review, the processes that are not easy to predict using RANS but are so using LES are highlighted. Subsequently, the LES results for heat transfer and conjugate heat transfer in the rib, for which experimental data are scarce, are summarized. Next, LES data on the rotation effect and rib geometry of the internal cooling passage are reviewed [3,5]. Finally, the future direction for research using LES to analyze the cooling passage of a gas turbine is covered.

Table 1. The simulation conditions for performing LES analysis of ribbed channels by research institution.

Institution	Country	Year [Ref]	Software	Reynolds Number	ple	e/H	Aspect Ratio	Rib Geometry
Tokyo Univ. Agriculture and Mechanics	Japan	2000 [25]	In-house	4000–9000	10	0.1	1, 2, 4	90°
		2001 [26]	In-house	1000, 4000	10	0.1	1	60°, 90°
		2001 [27]	In-house	4000	10	0.1	1	60°, 90°
		2001 [28]	In-house	4000	10	0.1	1	60°, 90°
		2003 [29]	In-house	4000	10	0.1	0.25, 1, 4	60°, 90°
		2004 [30]	In-house	4000	10	0.1	1	60°, 90°
		2004 [31]	In-house	4000	10	0.1	1	60°, 90°
		2008 [32]	In-house	1000, 4000	10	0.1	1	60°

Table 1. Cont.

Institution	Country	Year [Ref]	Software	Reynolds Number	p/e	e/H	Aspect Ratio	Rib Geometry
Denken	Japan	2002 [33]	In-house	100,000	10	0.1	∞	90°
		2005 [34]	In-house	50,000	10	0.1	2	60°
Univ. Iowa	USA	2003 [35]	In-house	10,020	1, 5, 10	0.1	∞	90°
Iowa State Univ.	USA	2004 [36]	In-house	5600	10	0.2	∞	90°
Virginia Tech	USA	2004 [37]	In-house	20,000	10	0.1	1	90°
		2005 [38]	In-house	20,000	10	0.1	1	90°
		2006 [39]	In-house	20,000	10	0.1	1	90°
		2006 [40]	In-house	20,000	10	0.1	1	90°
		2006 [41]	In-house	20,000	10	0.1	1	90°
		2008 [42]	In-house	20,000	10	0.1	1	90°
		2018 [43]	In-house	100,000	10	0.1	1	90°
		2021 [44]	In-house	10,000	10	0.3		90°
		2021 [45]	In-house	20,000	10	0.1	1	90°, BS, FS
		2022 [46]	In-house	20,000	10	0.1	1	90°, BS, FS
Seoul Nat'l Univ.	Republic of Korea	2005 [47]	In-house	30,000	10	0.1	∞	90°, semicircle
		2007 [48]	In-house	30,000	10	0.1	∞	90°
		2010 [49]	In-house	30,000	10	0.1	∞	90°, detached
Louisiana State Univ.	USA	2005 [50]	In-house	12,500	10	0.1	1	90°
		2005 [51]	In-house	25,000	10	0.1	0.25, 1, 4	90°
		2007 [52]	In-house	25,000, 100,000	10	0.1	0.25, 1, 4	90°
Cambridge	UK	2005 [53]	In-house	14,200	20	0.1	1	90°
		2015 [54]	In-house	20,000	10	0.1	1	90°
		2021 [55]	In-house	14,200	20	0.1	1	90°
Von Karman Institute	Belgium	2006 [56]	Fluent6.1	40,000	10	0.3	1	90°
		2015 [57]	In-house	40,000	10	0.3	1	90°
		2016 [58]	In-house	40,000	10	0.3	1	90°
IIT	India	2012 [59]	In-house	2053	10	0.1	1	90°
Univ. Manchester	UK	2015 [12]	In-house	30,000	9	0.1	∞	90°
Sapienza Univ. Roma	Italy	2015 [60]	In-house	15,000	10	0.1	1	90°
		2017 [61]	In-house	15,000	10	0.1	1	90°
ONERA	France	2016 [62]	In-house	40,000	10	0.3	1	90°
Peking Univ.	China	2016 [63]	In-house	30,000	9	0.1	1	90°
Univ, Manitoba	Canada	2015 [64]	PIV	13,000	8	0.1	1	90°, V(30,45,60°)
		2017 [65]	In-house	5600	8	0.1	1	90°, V(45,60°)
		2021 [66]	In-house	5600	8	0.1	1	90°

Table 1. Cont.

Institution	Country	Year [Ref]	Software	Reynolds Number	p/e	e/H	Aspect Ratio	Rib Geometry
Niigata Univ.	Japan	2016 [67]	In-house	5000	2, 4, 8, 16	0.1	∞	90°
		2020 [68]	In-house	5000	2, 4, 8, 16	0.1	∞	90°
Kookmin Univ.	Republic of Korea	2017 [69]	In-house	30,000	10	0.1	∞	90°
		2021 [10]	In-house	30,000	10	0.1	∞	90°
		2021 [70]	In-house	30,000	10	0.1	∞	90°
		2022 [71]	In-house	30,000	10	0.1	∞	90°
Univ. Stuttgart	Germany	2018 [72]	o-FOAM	30,000	10	0.1	1	
Karlsruhe Institute of Tech.	Germany	2018 [73]	Fluent v.15	100,000	10	0.1	1	90, V(60°)
CEFRACS	France	2020 [74]	In-house	15,000	10	0.1	1	90°
		2021 [75]	In-house	15,000	10	0.1	1	90°

PIV: particle image velocimetry; BS: backward step; FS: forward step.

2. Numerical Challenges and Comparative Studies

In the 50 papers analyzed in this review paper (see Table 1), the governing equations comprise the following incompressible Navier–Stokes equations and energy equations [10].

$$\frac{\partial \bar{u}_i}{\partial x_i} = 0 \quad (1)$$

$$\frac{\partial \bar{u}_i}{\partial t} + \frac{\partial \bar{u}_i \bar{u}_j}{\partial x_j} = -\frac{d\bar{p}}{dx_i} + \frac{1}{\text{Re}} \frac{\partial^2 \bar{u}_i}{\partial x_j \partial x_j} + \frac{\partial \tau_{ij}}{\partial x_j} \quad (2)$$

$$\frac{\partial \bar{\theta}}{\partial t} + \frac{\partial}{\partial x_j} (\bar{u}_j \bar{\theta}) = \frac{1}{\text{Re Pr}} \frac{\partial^2 \bar{\theta}}{\partial x_j \partial x_j} + \frac{\partial q_j}{\partial x_j} \quad (3)$$

where the over bars refer to the grid-filtered quantities of LES, while τ_{ij} and q_j are the stress and heat flux at the sub-grid scale (SGS), respectively. The parts that need to be modeled in the LES: τ_{ij} is usually modeled as being proportional to the velocity gradient for which currently, either a constant value is used or it is determined by considering conditions such as the flow or wall [76].

Although compressible flow is sometimes considered in the LES of film cooling [77], the internal cooling passage is simulated as incompressible flow by using the above equations. Although there is a problem with the convection term becoming unstable when simulating film cooling, which is an external flow [78], this does not occur when analyzing a ribbed channel, which is an internal flow. In addition, periodicity is often imposed in simulations of fully developed flows in ribbed channels. When developing a flow that is not sensitive to inflow, there is no inflow generation issue appearing during film cooling [78].

Commercial packages such as Fluent have been mainly used for LES of film cooling [78], but as summarized in Table 1, in-house codes have been mainly used for LES studies of ribbed channels. The Reynolds number was lower than that of actual gas turbines in the early 2000s, but recently LES was performed in the range of 10,000 to 100,000, which is a typical value for gas turbines. Blockage ratio ($=e/H$) and pitch ratio ($=p/e$) are mostly 0.1 and 10, respectively. The most common rib angle is 90°, and some LES for angled ribs are also being performed.

Ribbed channel flow has other considerations not applicable to film cooling. First, to impose cyclic boundary conditions at the inlet and outlet in a fully developed flow, the

streamwise pressure drop and heat transfer must be corrected. This is solved by decoupling the mean pressure and temperature gradient, as is shown in the following equations [79]:

$$P(\mathbf{x}, t) = -\beta x + p(\mathbf{x}, t) \quad (4)$$

$$T(\mathbf{x}, t) = \gamma x + \theta(\mathbf{x}, t), \quad (5)$$

where β and γ are the mean streamwise gradients of the pressure and temperature, the determination of which satisfies the conservation of global momentum and energy, respectively [79].

Second, there is a sharp edge in the rib that can cause wiggle in the data near the upstream edge [36] or it may become difficult to construct a body-fitted grid. Since LES data are rougher than RANS data, this numerical instability can be solved by increasing the grid resolution: it takes around 1 million grids to solve one periodic box and approximately 10 million grids to solve one passage in a ribbed channel [20,21].

The author of [38] compared quasi-direct numerical simulation (DNS) data performed in the same grid system with LES data by adopting the dynamic SGS model [80] in a ribbed duct, which showed a difference of 10% to 15% in heat transfer prediction. The authors of [64] also showed that LES, course-grid LES, and detached eddy simulation (DES) similarly predicted local heat transfer. Most of the research teams in Table 1 adopted the dynamic SGS model, albeit the SGS turbulent viscosity value obtained using scale similarity may be unstable. To solve this problem, a method of averaging while tracking flow particles [81] was proposed, while local averaging [82] has often been used in ribbed channel studies.

Unlike using RANS, LES consistently predicts the flow and heat transfer characteristics of ribbed channels [20,21]. Looking at the time-averaged streamlines presented in Figure 2b, the two LES data examples predict the location of the reattachment point similarly to the particle image velocimetry (PIV) data [11]. When using RANS, although there are slight differences depending on the model, the reattachment point is generally predicted to appear slightly downstream from the experimental value.

Figure 3 shows a comparison of the results for local heat transfer in the channel wall between ribs predicted by using RANS and LES. It has been reported that local heat transfer predictions using RANS differ by up to 250% depending on the model [20,21], as demonstrated in Figure 3a. The k - ϵ shear stress transport (SST) and Spalart–Allmaras (SA) models greatly underpredict heat transfer, while the other models predict the local heat transfer distribution differently.

Figure 3b shows three comparisons of LES data with experimentally obtained results. The three sets of experimental data were obtained using TLC [47], naphthalene sublimation [85], or laser holography [86]. In all three, the first peak appears at $3 < x/e < 4$ while the second peak appears before $x/e = 9$. The LES results obtained by the three different groups provided predicted local peaks that converge within a much narrower range than the RANS data in Figure 3a.

The difference between the LES and RANS data for ribbed channel flow is more evident in the turbulence data in Figure 4 than in the time-averaged velocity field in Figure 2b. With LES, the turbulent kinetic energy (TKE) appears high in the shear layer from the top surface of the rib to the downstream, which is not predicted by the k - ω SST model at all. Although the v^2 - f model predicts high TKE of the shear layer to some extent, it predicts the location where the maximum TKE occurs differently than when using LES.

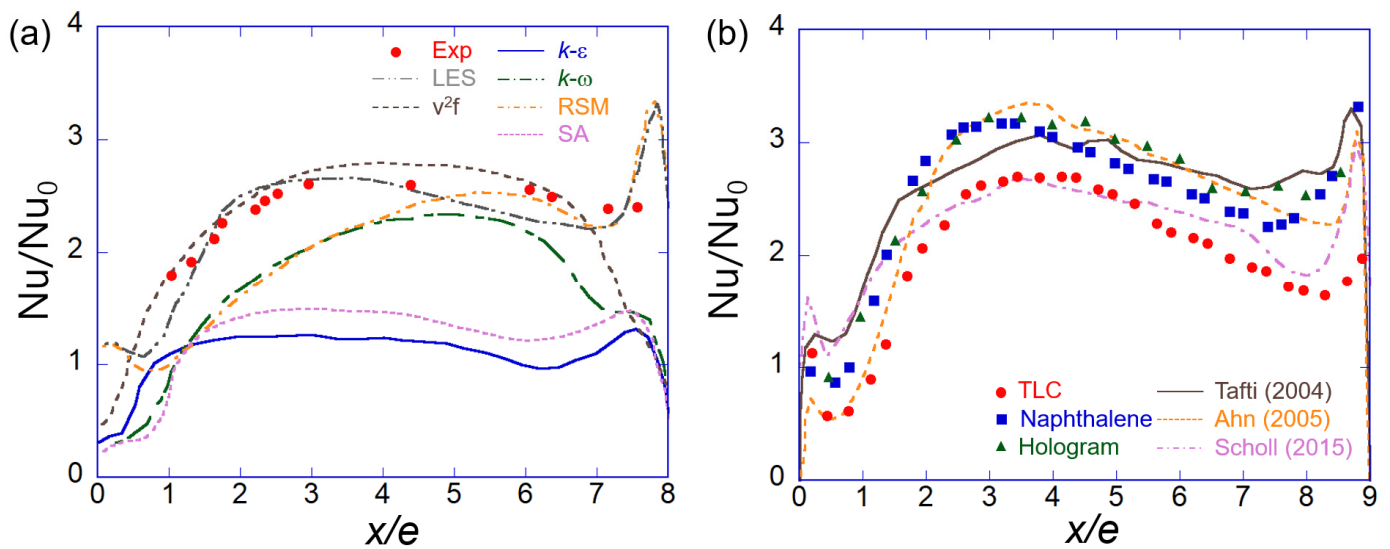


Figure 3. The local Nusselt number distribution on the channel wall between the ribs; (a) RANS data [12] (v^2f from [83]) compared to experiment [84]; (b) Three experiments [47,85,86] and three LES data [38,47,57]. SA: Spalart–Allmaras.

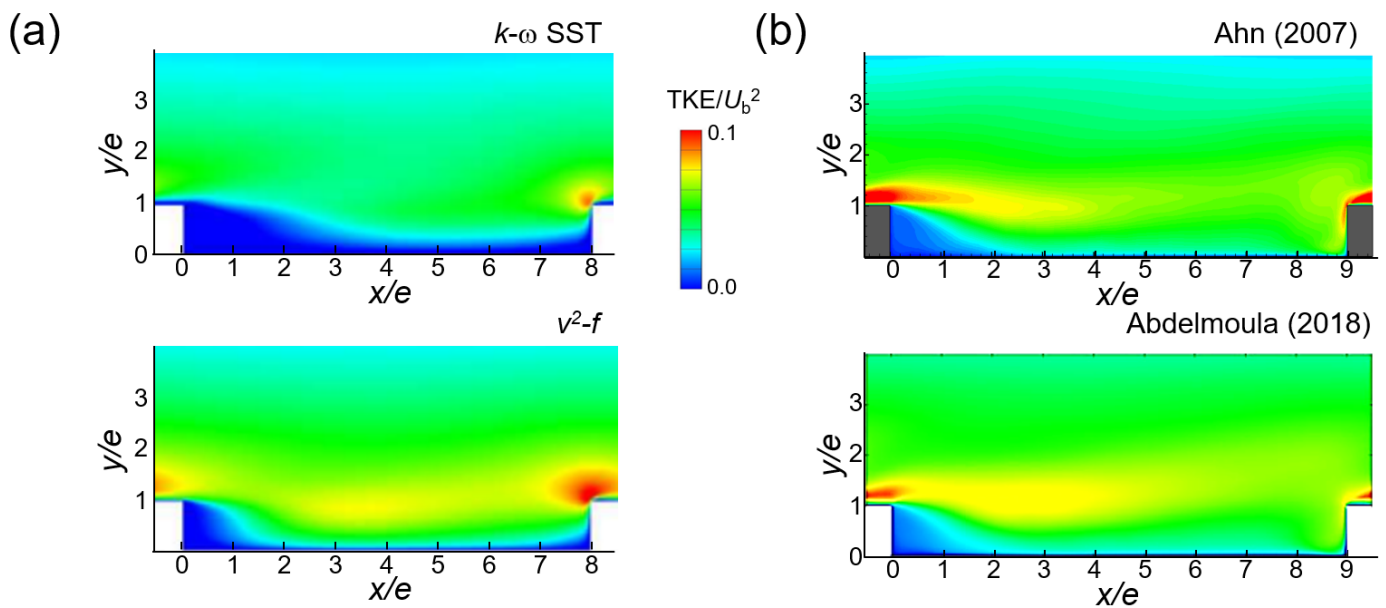


Figure 4. Turbulent kinetic energy (TKE) contours; (a) RANS data [12]; (b) LES data [48,72].

3. Instantaneous Flow and Thermal Fields

The local heat transfer in Figure 3b can be explained by the flow field in Figure 2b [86]. The first peak appearing at $3 < x/e < 4$ can be accounted for by reattachment of the separated flow; the reattachment point in Figure 2b is around $4 < x/e < 5$, and there is a slight difference in location. The second peak occurring before $x/e = 9$ can be explained by the influence of a corner vortex. However, although one appears in front of the rib in the RANS data in Figure 2b, the second peak is not clear except for the Reynolds stress model (RSM) of the heat transfer data in Figure 2a.

The above issues can be explained in terms of the instantaneous flow and temperature fields obtained using LES. When comparing the vector plot and temperature contour in Figure 5a, it can be seen that shear layer vortices are generated downstream of the rib while the cold main flow is introduced so that the heat transfer peak occurs upstream of the reattachment line. The second peak can be explained by looking at the flow field and

temperature field near the channel wall shown in Figure 5b. Around $z/e = 4.5$ before $x/e = 9$, the velocity vector spreads to both sides along the rib as the reattached flow collides with the rib, and the blue streak spreads to both sides in the temperature field at that location. This impinging flow creates a second heat transfer peak.

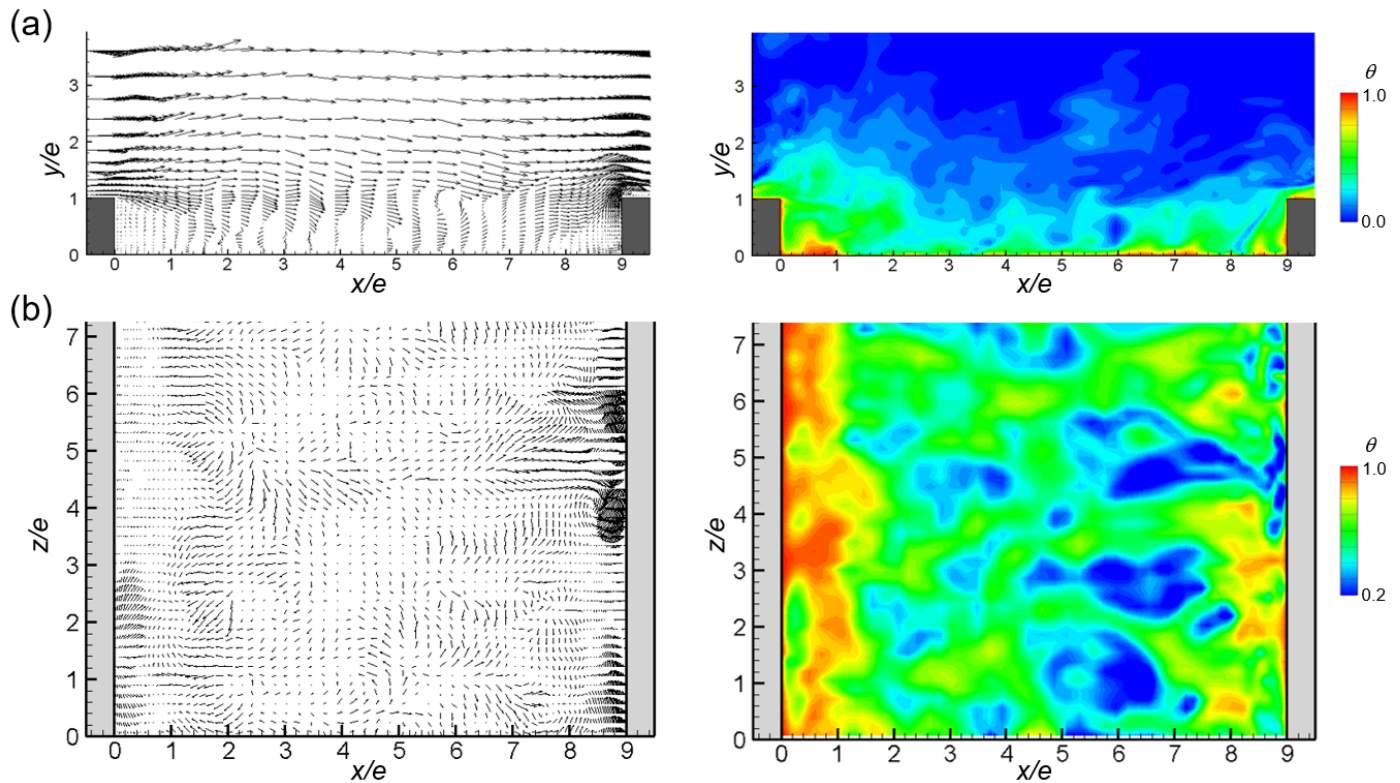


Figure 5. Instantaneous flow and thermal fields: (a) in the xy plane; (b) in the xz plane at $y/e = 0.06$.

Instantaneous flow field and temperature field information is limited to a specific moment and can be selective, so statistical verification is also being performed. The authors of [55] performed proper orthogonal decomposition (POD), thereby showing that 80 modes exist. Meanwhile, [75] performed dynamic mode decomposition (DMD), thereby showing that there are dominant modes in the downstream and inter-rib ribs and that minor modes are also involved in heat transfer.

4. Heat Transfer on the Rib

The heat transfer promotion of the rib turbulator peaks in front of the reattachment point and weakens downstream, so the ribs are installed periodically in the flow direction [1]. The installation spacing (p) of the ribs is usually around 10 times their height (e). In this case, if the cross-section of the rib is square, its surface area accounts for 25% of the heat transfer area. Since the heat transfer rate of the rib is expected to be higher than that of the channel wall, information on the heat transfer through the rib is very important for the design of the cooling passage. However, most of the heat transfer results for the ribbed channel were determined at the channel wall only [18].

The authors of [18] could not identify the details of the heat transfer on the surface of the rib by using thermocouple data, and since access from the front and back of the rib for optical measurement apparatus such as TLC or using infrared cameras is difficult, measurement data are rare [3,15]. The authors of [86] measured the heat transfer data on the rib surface by obtaining laser holography images from the side of the test section, while [87] measured the heat transfer distribution on the rib surface by securing optical access from the high blockage rib. The heat transfer distribution on the rib surface can be obtained using CFD, and LES provides more reliable data than RANS.

Figure 6 shows a comparison of the heat transfer on the rib obtained using LES and obtained experimentally. Compared with the channel wall in Figure 3b, the deviation between the data is large. Among the three surfaces of the rib, the front one has the largest Nusselt number ($0 < s/e < 1$). Although the LES results predict a sharp heat transfer peak at the upstream edge, this is not clear from the experimental data.

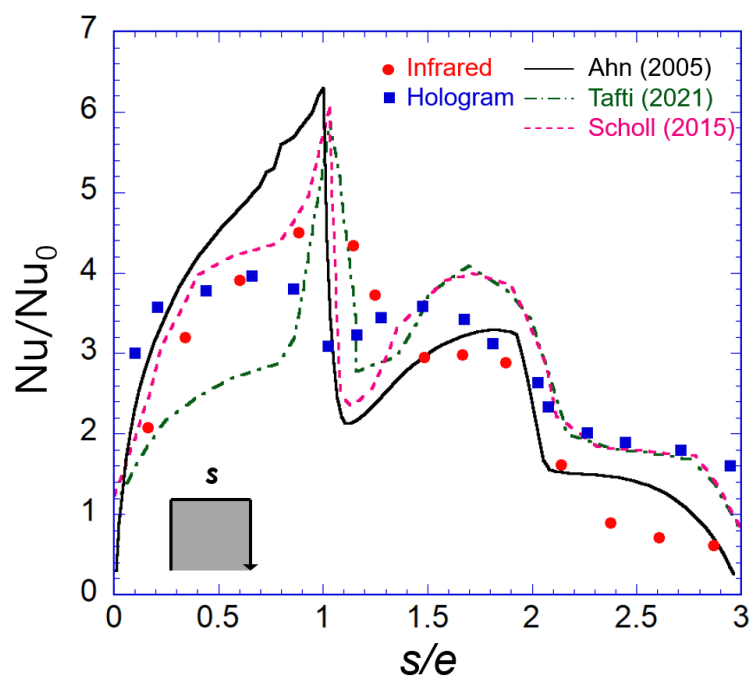


Figure 6. Local heat transfer distribution on the rib (2 experiments [86,87] and 3 LES data [44,47,57]).

At the top surface ($1 < s/e < 2$), the flow detached from the upstream edge becomes reattached (Figure 2b), resulting in a heat transfer peak at $1.5 < s/e < 2$, which is commonly predicted by using the three sets of LES results and the experimental data in [87]. Meanwhile, only the results in [86] with measurements obtained by using a laser hologram do not follow this trend. Heat transfer at the rear surface ($2 < s/e < 3$), which is the weakest among the three surfaces, decreases from the edge to the corner. This trend is unanimous when comparing the five datasets in Figure 6.

5. Conjugate Heat Transfer

The rib installed in the cooling passage of the gas turbine also serves as a fin to widen the heat transfer area. To obtain accurate measurements of the heat transfer performance, the fin performance while considering the thermal conduction from the rib must be obtained [88,89]. To perform this, it is necessary to find the temperature inside the rib. Since it is difficult to plant a sensor inside the rib in experiments, it is obtained by measuring the temperature distribution on the surface and performing a separate conduction analysis using this as a boundary condition [89].

In CFD, conjugate heat transfer simulation including thermal conduction must be performed. The authors of [88] analyzed the conjugate heat transfer of the ribbed channel using RANS, but did not consider the conduction at the channel wall. When trying to analyze the conjugate heat transfer for a ribbed channel with LES, a problem arises in that the time scales of conduction and convection are significantly different. The authors of [58] solved this by exchanging time-averaged boundary conditions intermittently while applying separate solvers for solids and fluids. The authors of [10,44] performed a fully coupled analysis by applying the immersed boundary method.

Figure 7a shows a comparison of the temperature distribution after conjugate heat transfer analysis with that of pure convection. Since the thermal conductivity of gas

turbine materials is around 600 times that of cooling air [10,89], the solid interior is close to isothermal and most of the temperature change occurs inside the rib. Therefore, the height of the rib [10] is better than the thickness of the channel wall for use as the characteristic length in the Biot number calculation [90] until the thermal conductivity decreases, at which point the latter becomes more appropriate [70].

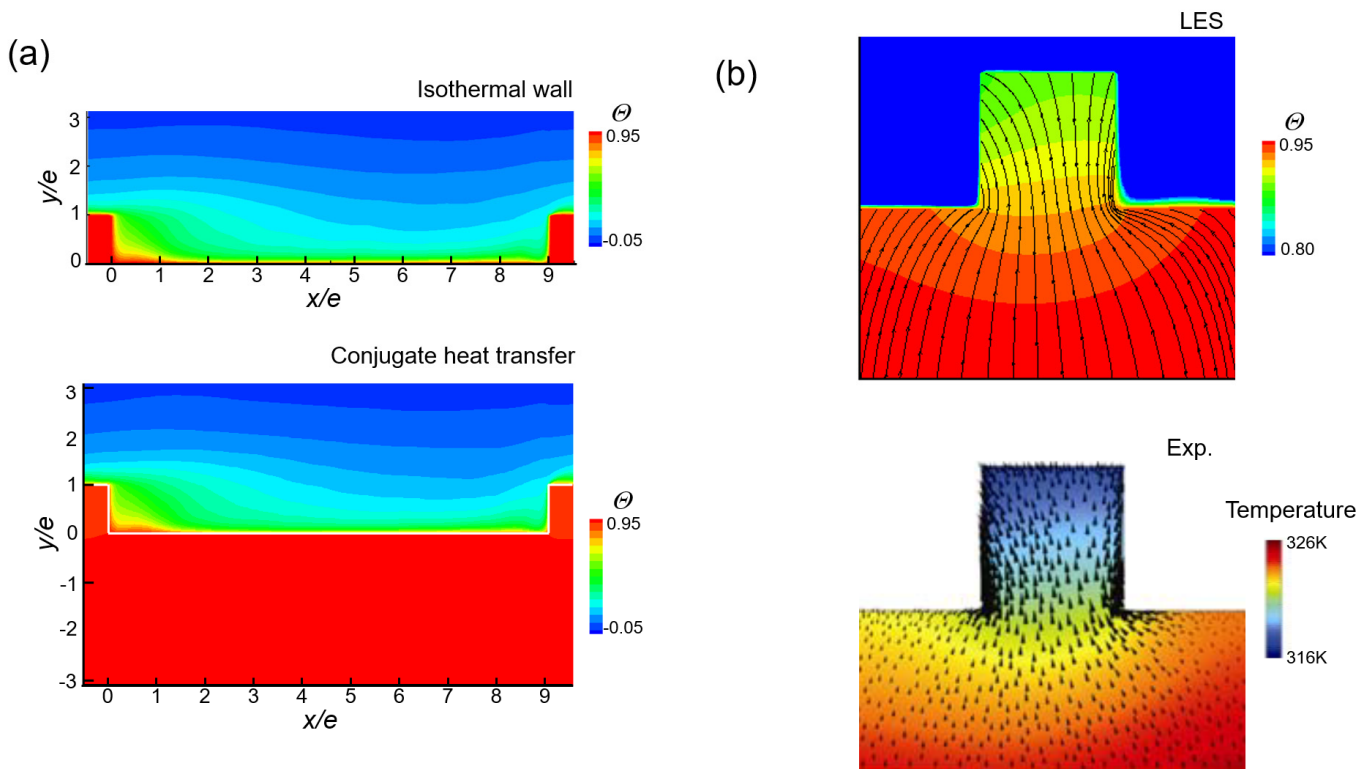


Figure 7. Thermal fields in a ribbed channel with a conducting wall [10]: (a) temperature contours in the xy plane; (b) the temperature around the rib.

Figure 7b depicts a comparison of the temperature distribution inside the rib obtained by LES with experimentally obtained results; the temperature distribution and heat flux vector obtained by using LES and experimentally are in good agreement. Moreover, it can be seen that the channel wall should be included in the analysis because of the effect of the heat conduction from the rib penetrating the channel wall.

Figure 8a shows a comparison of the heat transfer data in a conducting channel wall obtained experimentally and via LES. At the channel wall, the effect of conduction is not significant, so the conjugate heat transfer data appears similar to the iso-flux data. In the experiment, the conjugate data [89] (blue squares) occur sooner after the rib ($0 < x/e < 2$) and in front of the rib ($8 < x/e < 9$) than the iso-flux data (red circles) [87]. However, this trend cannot clearly be seen in the LES results. Although this tendency is evident in [10], the blockage ratio is different, so additional investigations are needed.

Figure 8b illustrates a comparison of the heat transfer on the rib surface. Compared with the iso-flux data (red circles), the conjugate data (blue square) show a decrease in heat transfer at the front surface ($0 < s/e < 1$) and the rear surface ($2 < s/e < 3$). Although a decrease in heat transfer at the rear surface was predicted by [44], a change at the front surface was not clearly observed in the LES data. The authors of [44,57,58] performed LESs under the same conditions and shapes as the experiments performed by [87,89], so the difference in the heat transfer at the front surface seems to be due to the difference in the time scales for conduction and convection.

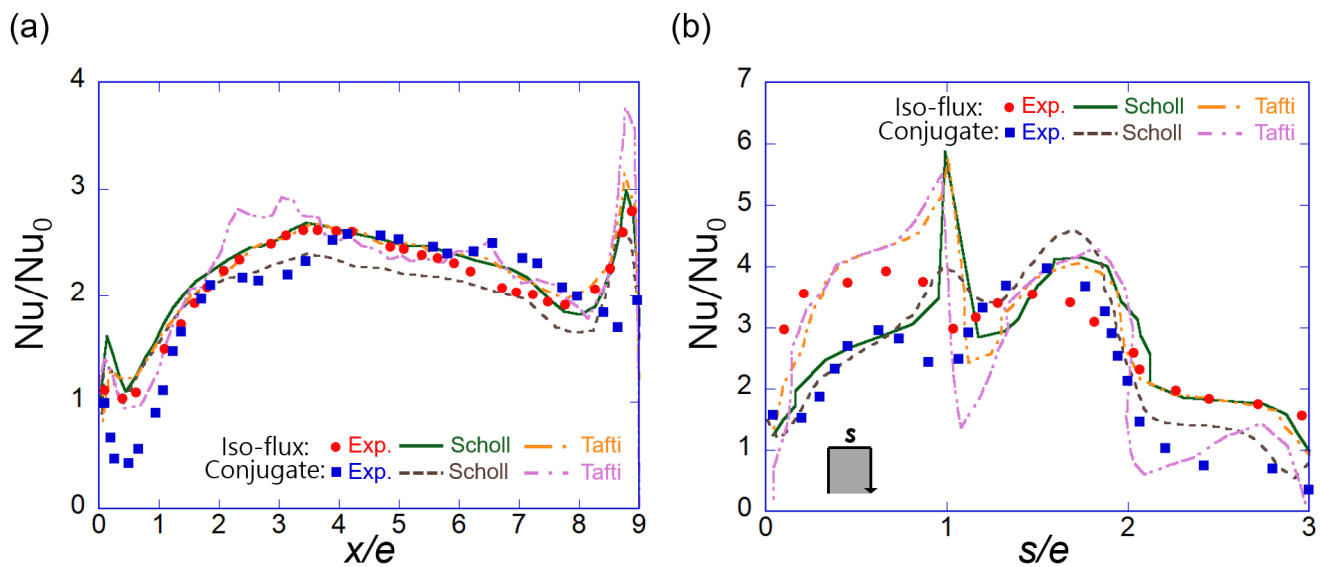


Figure 8. Local heat transfer distributions: (a) on the channel wall; (b) on the rib. The experimental data [87,89] are represented by symbols and the LES data [44,57,58] by lines.

6. The Effects of Rotating the Gas Turbine Blade

Rotating the gas turbine blade affects the heat transfer in the cooling channel [3,4], and since it is difficult to measure this experimentally, CFD can be usefully employed instead. However, the effects of rotation are not well-represented in RANS [36,48], so LES was identified as being more suitable for examining this phenomenon. In LES, the centrifugal force or rotating buoyancy effect of using a high rotation speed can be implemented more easily than can be achieved experimentally [42,50].

As shown in Figure 9a, to test the heat transfer of the rotating ribbed duct, the duct and the sensor including the camera must be rotated together and the balance must be well-matched to obtain a high rotation number [3]. The experimental results in Figure 9b show that the heat transfer characteristics change by rotation. However, rotational buoyancy caused by rotation with centrifugal force is difficult to observe experimentally.

The local heat transfer distribution of the rotating ribbed channel obtained by LES is presented in Figure 9c,d. The rotation effect not well-predicted by using RANS can be by using LES. Heat transfer is promoted in the trailing wall when LES is used with an Ro value of 0.3 (Figure 9c) [48,50], which could not be obtained experimentally by [91]. The results from [48,50] agree well in Figure 9c even though the channel aspect ratio is different (see Table 1).

Although heat transfer can be seen to decrease at the leading wall in Figure 9d, LES underpredicts the amount of heat transfer reduction for $Ro = 0.1$. The data in [50] show a significantly different distribution from other LES or experimentally obtained data. The heat transfer at the leading wall appears to be more sensitive to the channel aspect ratio than that at the trailing wall (see Table 1). When replacing the test duct in the rotation rig in Figure 9a, the sensor must be installed and the balance must be re-adjusted. Thus, LES is a useful tool for studying the rotation effect according to the duct aspect ratio.

Rotating buoyancy, which is difficult to experimentally implement close to that in a real gas turbine, can be imposed by using LES. Around 1 million grids are required to analyze one cycle in the flow direction of a ribbed channel using LES, while tens of millions of grids are required to analyze a two-pass duct [20,21]. Due to recent improvements in hardware performance, data on a two-pass duct can be obtained via LES (Figure 10) [43].

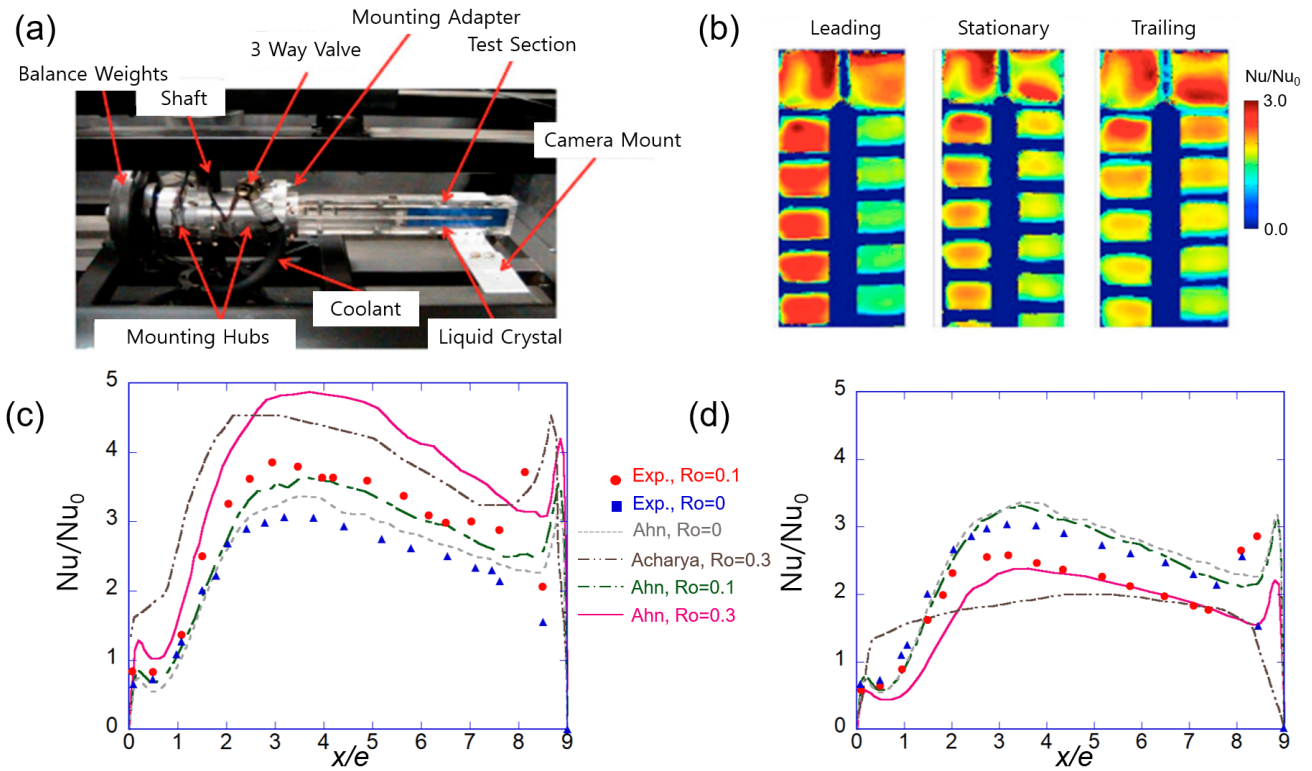


Figure 9. Heat transfer in the rotating ribbed channel: (a) A typical experimental setup [3]; (b) local heat transfer distributions [3]; (c) the local Nusselt number on the trailing wall; (d) the local Nusselt number on the leading wall. Ro : rotation number (LES data [48,50] compared to experiment [91]).

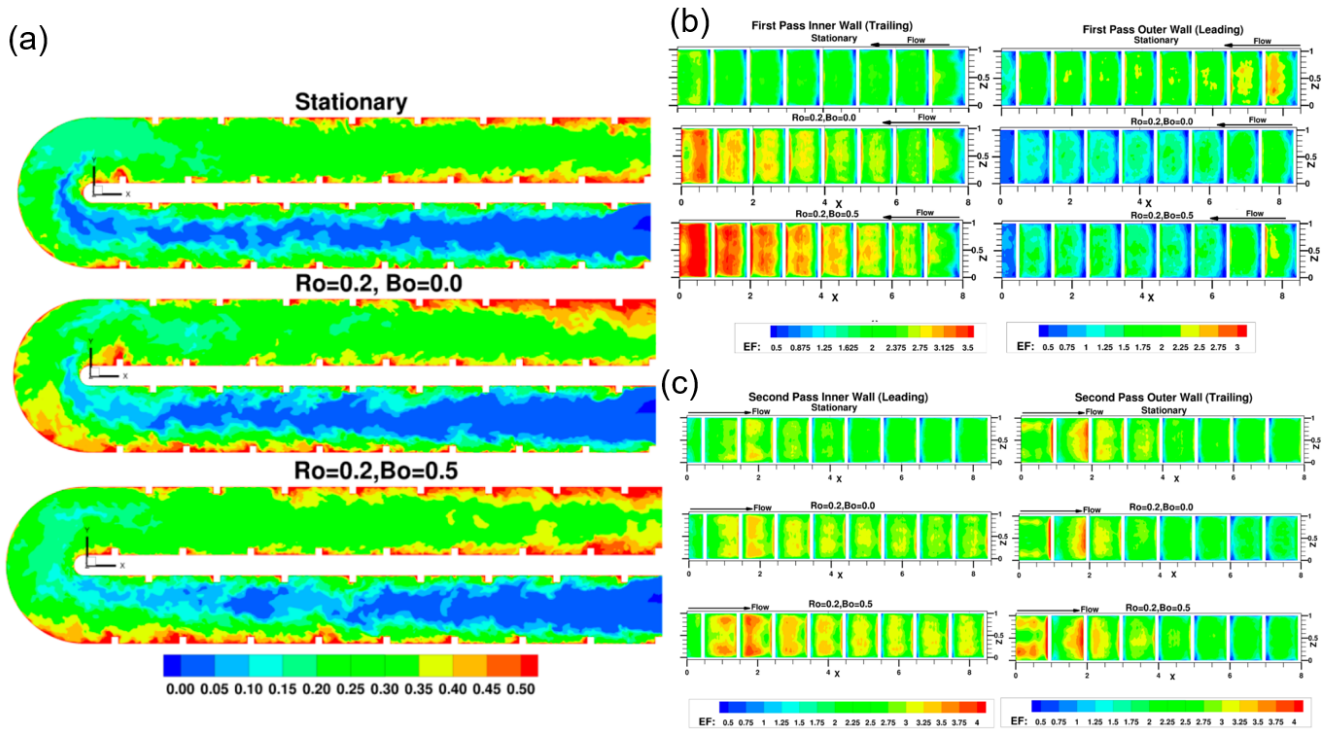


Figure 10. Large eddy simulation of heat transfer in a two-pass rotating ribbed duct [43]: (a) thermal fields in the channel; (b) heat transfer on the channel wall during the first pass; (c) heat transfer on the channel wall during the second pass. Bo : buoyancy number.

In Figure 10a, it can be seen that the effect of buoyancy number appears downstream in the first pass where the coolant is heated in the second pass. In the heat transfer distribution of the first pass shown in Figure 10b, the entry effect appears to be common and both the rotation effect and the buoyancy effect occur. The effect of a sharp 180° turn occurs during the heat transfer in the second pass (Figure 9c). Many studies have been conducted on shapes to secure flow uniformity during sharp 180° turns [92], for which LES is a useful tool that will be widely used in such studies.

7. Geometrical Shapes for Performance Improvement

Although a rib turbulator installed in the internal cooling passage of a gas turbine promotes heat transfer, it also causes additional pressure loss. In addition, heat transfer becomes locally non-uniform, especially in the low heat transfer region behind the rib. To improve this problem, various rib shapes have been proposed [1], as shown in Figure 11. Since the gas turbine blade has an airfoil-shaped cross-section, those in the cooling passage near the leading edge and trailing edge are semicircular or triangular, respectively (see Figure 11). In most studies on gas turbine internal flow channels, the researchers have dealt with the effects of the geometric parameters on heat transfer and pressure drop [1].

- transverse, angled, compound angled, V-shaped, W-shaped, discrete ...

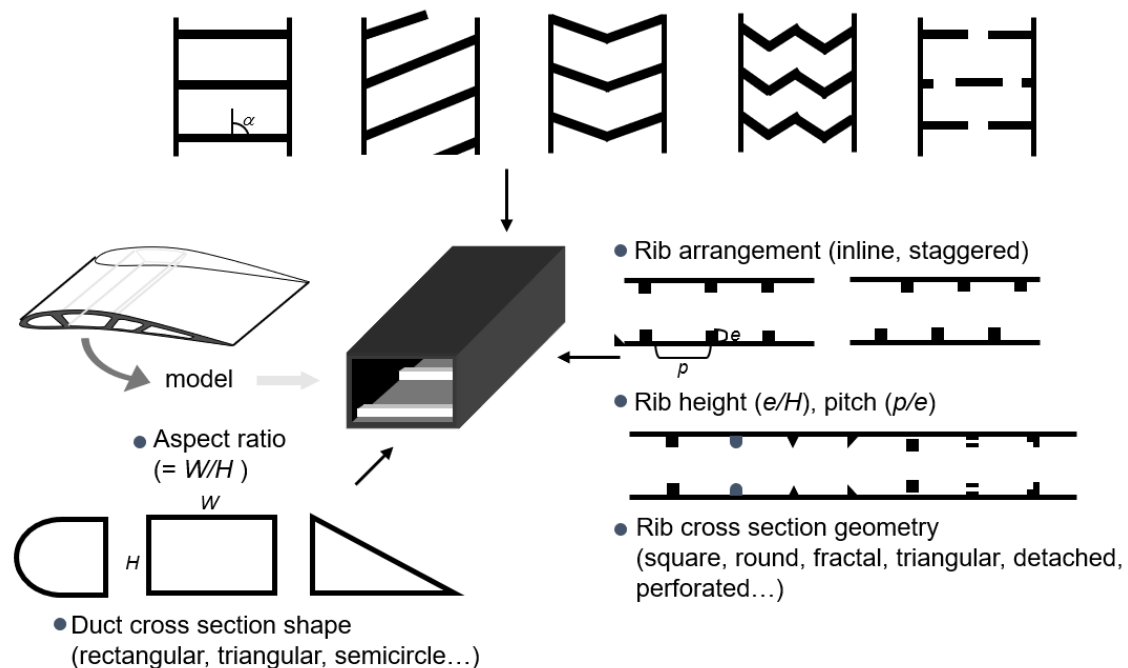


Figure 11. Geometrical shapes and variables affecting heat transfer in the internal cooling passage of a gas turbine.

The shape of ribs, especially ribs angled as V and W shapes, has been actively studied over the past 40 years, with articles on the subject being published recently [93]. When the rib is at an angle to the main flow, the secondary flow is generated in the duct to promote heat transfer. Compared with using transverse ribs, the latter can be relatively well-predicted by using RANS and the results are in good agreement with the experimentally obtained ones. The authors of [94] performed RANS under the same conditions as used in the experiment in [95] and obtained a local heat transfer distribution profile similar to the experimentally obtained one (Figure 12).

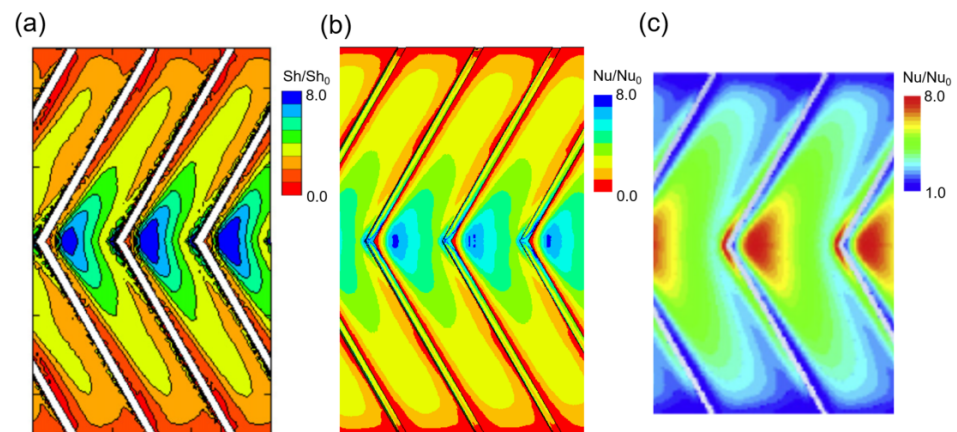


Figure 12. Local heat transfer distribution on a channel wall with V-shaped ribs: (a) experimental data [95]; (b) RANS data with RSM [94]; (c) RANS data with the k -model [96].

Comparing Figure 12a,b demonstrates that heat transfer is underpredicted compared with the experiment and the reattachment point is pushed slightly downstream, so obtaining better results with LES remains possible. The k - ϵ model, which does not predict heat transfer in the transverse rib well, also provides a heat transfer distribution close to the experimentally obtained one when using V-shaped ribs, as shown in Figure 12c. When performing LES on a model using angled ribs, the Reynolds number in [26] is rather low whereas that in [55] is over 10,000. Meanwhile, although [73] performed DES for V-shaped ribs and obtained results in good agreement with the experimentally obtained ones, they could not provide instantaneous large flow structures. Moreover, [64,65] performed LES but did not include heat transfer.

The most studied topic for rib geometries is their cross-sectional shape [97,98]. Figure 13a shows a comparison of the streamlines obtained in channels with semicircular ribs and detached ribs by using LES. The semicircular rib shows a flow structure similar to that of the square rib, and the heat transfer distribution comparison shown in Figure 13b is also similar [47]. The detached rib promotes heat transfer in the low heat transfer region behind the rib [99], albeit the heat transfer promotion effect decreases near the reattachment point (Figure 13b) [49].

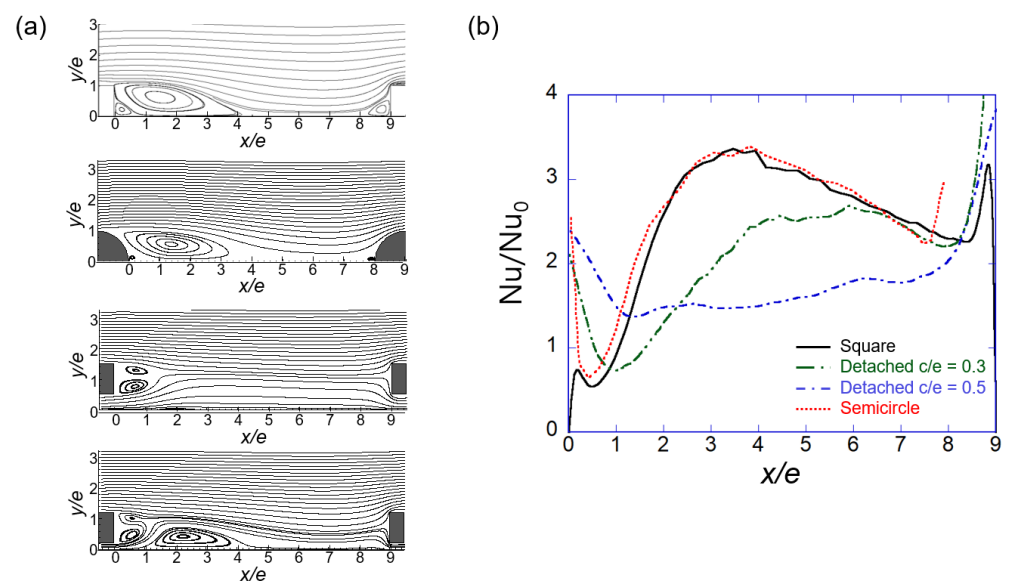


Figure 13. Effects of rib cross-section geometry on flow and heat transfer in a ribbed channel [47,49]; (a) time-averaged streamlines; (b) local heat transfer distributions on the channel wall.

The authors of [97] performed RANS on 16 different rib cross-sectional shapes and presented data with the best heat transfer performance for boot-type ribs with the downstream side shaved off. The authors of [45] recently performed LES on the forward step rib and the backward step rib, and the backward step rib obtained better heat transfer performance. The authors of [55] performed LES on 10 rib cross-sections and obtained good heat transfer performance in the shape where the downstream side of the rib was shaved as in [97].

8. Conclusions

Herein, 50 studies published over the past 20 years on the flow and heat transfer in a ribbed channel by simulating the flow path inside a gas turbine using LES are reviewed. The main findings can be summarized as follows.

In ribbed channel flow, instability in the convection term or inflow generation problem does not appear, so LES can be performed more easily than with film cooling. The effect of the SGS model on the heat transfer results is not significant, and the LES results obtained by several groups are very consistent, unlike those obtained using RANS. Including sharp corners in the geometrical shape of the ribs causes grid configuration and stability issues. When considering the thermal conduction by the rib, there is a time scale difference between flow and conduction. An immersed boundary method that supports conjugate heat transfer has been used as a solution to these numerical problems.

LES can be used to not only accurately predict heat transfer in ribbed channels but also provide instantaneous flow and temperature field and turbulence statistics that using RANS cannot. Based on this information, it is possible to explain the local heat transfer distribution process and identify the mechanism that promotes heat transfer. In addition, LES provides local heat transfer distribution or conjugate heat transfer data for the ribs, for which there is a lack of experimentally obtained data. High rotation and buoyancy effects, which are difficult to measure experimentally, can also be simulated by using LES.

9. Future Directions

Improvements in computing hardware have enabled LES results to be obtained for two-pass ducts, and using LES to simulate the entire internal cooling passage is expected to be possible soon. Compared with the shape of the rib, not much data on duct geometry using LES have been published. It is anticipated that using LES for a triangular duct [100] appearing near the trailing edge or semicircular duct near the leading edge will be available soon. Problems with experimental high-resolution optical measurement methods can be overcome using LES, which thereby can make a useful contribution.

In addition to the duct geometry, heat transfer promoters such as dimples and pin fins are used near the trailing edge. LES results on using a dimpled channel have been published since 2008 [101,102], showing that LES can be used to predict local heat transfer much better than RANS. LES results on using pin fins have recently begun to be published [103], while research including conjugate heat transfer will be needed in the future. Besides ribs, impinging jets and vortices are also widely used [104], so LES models including these should provide useful data.

Funding: This work was supported by an Agency for Defense Development Grant funded by the Korean Government (UD220004JD).

Data Availability Statement: Data are contained within this article.

Conflicts of Interest: The author declares no conflict of interest.

Nomenclature

d	thickness of the channel wall [m]
D_h	hydraulic diameter of the channel [m]
e	rib height [m]
f	friction factor
h	heat transfer coefficient [W/m^2K]
H	channel height [m]
k_f	thermal conductivity of fluid [W/mK]
Nu	Nusselt number ($=h D_h/k_f$)
p	rib-to-rib pitch [m]
Pr	Prandtl number ($=\nu/\alpha$)
Re	bulk Reynolds number ($=U_b D_h/\nu$)
Ro	rotation number ($=\omega D_h/U_b$)
q	heat transfer rate [W]
t	time [s]
T	temperature [K]
T_b	bulk temperature [K]
T_w	wall temperature [K]
U_b	bulk velocity [m/s]
W	channel width [m]
Greek symbols	
α	thermal diffusivity [m^2/s]
ν	kinematic viscosity [m^2/s]
θ	dimensionless temperature ($=(T - T_b)/(T_w - T_b)$)
Θ	time-averaged dimensionless temperature
Subscripts	
0	fully developed value in a smooth pipe

References

- Han, J.C. Advanced cooling in gas turbines 2016 Max Jakob memorial award paper. *J. Heat Transf.* **2018**, *140*, 113001. [\[CrossRef\]](#)
- Bunker, R.S. Gas turbine heat transfer: Ten remaining hot gas path challenges. *J. Turbomach.* **2017**, *129*, 193–201. [\[CrossRef\]](#)
- Ekkad, S.V.; Singh, P. Detailed heat transfer measurements for rotating turbulent flows in gas turbine systems. *Energies* **2021**, *14*, 39. [\[CrossRef\]](#)
- Yeranee, K.; Yu, R.A.O. A review of recent studies on rotating internal cooling for gas turbine blades. *Chin. J. Aeronaut.* **2021**, *34*, 85–113. [\[CrossRef\]](#)
- Ligrani, P. Heat transfer augmentation technologies for internal cooling of turbine components of gas turbine engines. *Int. J. Rotating Mach.* **2013**, *2013*, 275653. [\[CrossRef\]](#)
- Du, W.; Luo, L.; Jiao, Y.; Wang, S.; Li, X.; Sunden, B. Heat transfer in the trailing region of gas turbines—A state-of-the-art review. *Appl. Therm. Eng.* **2021**, *199*, 117614. [\[CrossRef\]](#)
- Chang, S.W.; Wu, P.-S.; Wan, T.-Y.; Cai, W.-L. A review of cooling studies on gas turbine rotor blades with rotation. *Inventions* **2023**, *8*, 21. [\[CrossRef\]](#)
- Takeishi, K. Evolution of turbine cooled vanes and blades applied for large industrial gas turbines and its trend toward carbon neutrality. *Energies* **2022**, *15*, 8935. [\[CrossRef\]](#)
- Alam, T.; Saini, R.P.; Saini, J.S. Heat and flow characteristics of air heater ducts provided with turbulators—A review. *Renew. Sustain. Energy Rev.* **2014**, *31*, 289–304. [\[CrossRef\]](#)
- Ahn, J.; Song, J.C.; Lee, J.S. Fully coupled large eddy simulation of conjugate heat transfer in a ribbed channel with a 0.1 blockage ratio. *Energies* **2021**, *14*, 2096. [\[CrossRef\]](#)
- Casarsa, L.; Arts, T. Experimental investigation of the aerothermal performance of a high blockage rib-roughened cooling channel. *J. Turbomach.* **2005**, *127*, 580–588. [\[CrossRef\]](#)
- Keshmiri, A.; Osman, K.; Benhamadouche, S.; Shokri, N. Assessment of advanced RANS models against large eddy simulation and experimental data in the investigation of ribbed passages with passive heat transfer. *Numer. Heat Transf. B* **2016**, *69*, 96–110. [\[CrossRef\]](#)
- Sharma, S.K.; Kalamkar, V.R. Computational Fluid Dynamics approach in thermo-hydraulic analysis of flow in ducts with rib roughened walls—A review. *Renew. Sustain. Energy Rev.* **2016**, *55*, 756–788. [\[CrossRef\]](#)
- Nidhul, K.; Yadav, A.K.; Anish, S.; Kumar, S. Critical review of ribbed solar air heater and performance evaluation of various V-rib configuration. *Renew. Sustain. Energy Rev.* **2021**, *142*, 110871. [\[CrossRef\]](#)

15. Ekkad, S.V.; Singh, P. Liquid crystal thermography in gas turbine heat transfer: A review on measurement techniques and recent investigations. *Crystals* **2021**, *11*, 1332. [[CrossRef](#)]
16. Jang, H.N.; Park, J.S.; Kwak, J.S. Experimental study on heat transfer characteristics in a ribbed channel with dimples, semi-spherical protrusions, or oval protrusions. *Appl. Therm. Eng.* **2018**, *131*, 734–742. [[CrossRef](#)]
17. Unnikrishnan, U.; Yang, V. A review of cooling technologies for high temperature rotating components in gas turbine. *Propuls. Power Res.* **2022**, *11*, 293–310. [[CrossRef](#)]
18. Taslim, M.E.; Wadsworth, C.M. An experimental investigation of the rib surface-averaged heat transfer coefficient in a rib-roughened square passage. *J. Turbomach.* **1997**, *119*, 381–389. [[CrossRef](#)]
19. Kumar, S.; Amano, R.S. An investigation in the numerical approach to solve the heat transfer phenomenon in gas turbine. *J. Energy Resour. Technol.* **2021**, *143*, 080805. [[CrossRef](#)]
20. Tyacke, J.C.; Tucker, P.G. Future use of large eddy simulation in aero-engines. *J. Turbomach.* **2015**, *137*, 081005. [[CrossRef](#)]
21. Tyacke, J.; Vadlamani, N.R.; Trojak, W.; Watson, R.; Ma, Y.; Tucker, P.G. Turbomachinery simulation challenges and the future. *Prog. Aerosp. Sci.* **2019**, *110*, 100554. [[CrossRef](#)]
22. Han, J.C.; Dutta, S. Recent developments in turbine blade internal cooling. *Ann. N. Y. Acad. Sci. USA* **2001**, *934*, 162–178. [[CrossRef](#)] [[PubMed](#)]
23. Yadav, A.S.; Agrawal, A.; Sharma, A.; Gupta, A. Revisiting the effect of ribs on performance of solar air heater using CFD approach. *Mater. Today Proc.* **2022**, *60*, 240–252. [[CrossRef](#)]
24. Iacovides, H.; Launder, B.E. Computational fluid dynamics applied to internal gas-turbine blade cooling: A review. *Int. J. Heat Fluid Flow* **1995**, *16*, 454–470. [[CrossRef](#)]
25. Murata, A.; Mochizuki, S. Large eddy simulation with a dynamic subgrid-scale model of turbulent heat transfer in an orthogonally rotating rectangular duct with transverse rib turbulators. *Int. J. Heat Mass Transf.* **2000**, *43*, 1243–1259. [[CrossRef](#)]
26. Murata, A.; Mochizuki, S. Comparison between laminar and turbulent heat transfer in a stationary square duct with transverse or angled rib turbulators. *Int. J. Heat Mass Transf.* **2001**, *44*, 1127–1141. [[CrossRef](#)]
27. Murata, A.; Mochizuki, S. Large eddy simulation of turbulent heat transfer in an orthogonally rotating square duct with angled rib turbulators. *J. Heat Transf.* **2001**, *123*, 858–867. [[CrossRef](#)]
28. Murata, A.; Mochizuki, S. Effect of centrifugal buoyancy on turbulent heat transfer in an orthogonally rotating square duct with transverse or angled rib turbulators. *Int. J. Heat Mass Transf.* **2001**, *44*, 2739–2750. [[CrossRef](#)]
29. Murata, A.; Mochizuki, S. Effect of cross-sectional aspect ratio on turbulent heat transfer in an orthogonally rotating rectangular duct with angled rib turbulators. *Int. J. Heat Mass Transf.* **2003**, *46*, 3119–3133. [[CrossRef](#)]
30. Murata, A.; Mochizuki, S. Centrifugal buoyancy effect on turbulent heat transfer in a rotating two-pass smooth square channel with sharp 180-deg turns. *Int. J. Heat Mass Transf.* **2004**, *47*, 3215–3231. [[CrossRef](#)]
31. Murata, A.; Mochizuki, S. Aiding and opposing contributions of centrifugal buoyancy on turbulent heat transfer in a two-pass transverse-or angled-rib-roughened channel with sharp 180 turns. *Int. J. Heat Mass Transf.* **2004**, *47*, 3721–3743. [[CrossRef](#)]
32. Murata, A.; Mochizuki, S. Effects of centrifugal buoyancy and Reynolds number on turbulent heat transfer in a two-pass angled-rib-roughened channel with sharp 180 turns investigated by using large eddy simulation. *Int. J. Rotating Mach.* **2008**, *2008*, 764720. [[CrossRef](#)]
33. Watanabe, K.; Takahashi, T. LES analysis and measurement of fully developed transverse ribbed channel flows and heat transfer. *Trans. Jpn. Soc. Mech. Eng. B* **2002**, *68*, 240–245. [[CrossRef](#)]
34. Watanabe, K.; Takahashi, T. LES and measurement of heat transfer and flow in rectangular channels with crossed angled ribs. *Trans. Jpn. Soc. Mech. Eng. B* **2005**, *17*, 1459–1464. [[CrossRef](#)]
35. Cui, J.; Patel, V.C.; Lin, C.L. Large-eddy simulation of turbulent flow in a channel with rib roughness. *Int. J. Heat Fluid Flow* **2003**, *24*, 372–388. [[CrossRef](#)]
36. Lee, J.S.; Meng, N.; Pletcher, R.H.; Liu, Y. Numerical study of the effects of rotation on heat transfer in channels with and without ribs. *Int. J. Heat Mass Transfer* **2004**, *47*, 4673–4684. [[CrossRef](#)]
37. Abdel-Wahab, S.; Tafti, D.K. Large eddy simulation of flow and heat transfer in a 90 deg ribbed duct with rotation: Effect of Coriolis and centrifugal buoyancy forces. *J. Turbomach.* **2004**, *126*, 627–636. [[CrossRef](#)]
38. Tafti, D.K. Evaluating the role of subgrid stress modeling in a ribbed duct for the internal cooling of turbine blades. *Int. J. Heat Fluid Flow* **2005**, *26*, 92–104. [[CrossRef](#)]
39. Sewall, E.A.; Tafti, D.K.; Graham, A.B.; Thole, K.A. Experimental validation of large eddy simulations of flow and heat transfer in a stationary ribbed duct. *Int. J. Heat Fluid Flow* **2006**, *27*, 243–258. [[CrossRef](#)]
40. Viswanathan, A.K.; Tafti, D.K. Detached eddy simulation of turbulent flow and heat transfer in a two-pass internal cooling duct. *Int. J. Heat Fluid Flow* **2006**, *27*, 1–20. [[CrossRef](#)]
41. Viswanathan, A.K.; Tafti, D.K. Detached eddy simulation of flow and heat transfer in fully developed rotating internal cooling channel with normal ribs. *Int. J. Heat Fluid Flow* **2006**, *27*, 351–370. [[CrossRef](#)]
42. Sewall, E.A.; Tafti, D.K. Large eddy simulation of flow and heat transfer in the developing flow region of a rotating gas turbine blade internal cooling duct with Coriolis and buoyancy forces. *J. Turbomach.* **2008**, *130*, 011005. [[CrossRef](#)]
43. Tafti, D.; Dowd, C.; Tan, X. High Reynold number LES of a rotating two-pass ribbed duct. *Aerospace* **2018**, *5*, 124. [[CrossRef](#)]

44. Oh, T.K.; Tafti, D.K.; Nagendra, K. Fully coupled large eddy simulation-conjugate heat transfer analysis of a ribbed cooling passage using the immersed boundary method. *J. Turbomach.* **2021**, *143*, 041012. [[CrossRef](#)]
45. Sreekes, K.; Tafti, D.K.; Vengadesan, S. Large-eddy simulation investigation of modified rib shapes on heat transfer in a ribbed duct. *J. Heat Transf.* **2021**, *143*, 112101. [[CrossRef](#)]
46. Sreekes, K.; Tafti, D.K.; Vengadesan, S. The combined effect of Coriolis and centrifugal buoyancy forces on internal cooling of turbine blades with modified ribs using large eddy simulation (LES). *Int. J. Therm. Sci.* **2022**, *182*, 107797. [[CrossRef](#)]
47. Ahn, J.; Choi, H.; Lee, J.S. Large eddy simulation of flow and heat transfer in a channel roughened by square or semicircle ribs. *J. Turbomach.* **2005**, *127*, 263–269. [[CrossRef](#)]
48. Ahn, J.; Choi, H.; Lee, J.S. Large eddy simulation of flow and heat transfer in a rotating ribbed channel. *Int. J. Heat Mass Transf.* **2007**, *50*, 4937–4947. [[CrossRef](#)]
49. Ahn, J.; Lee, J.S. Large eddy simulation of flow and heat transfer in a channel with a detached rib array. *Int. J. Heat Mass Transf.* **2010**, *53*, 445–452. [[CrossRef](#)]
50. Tyagi, M.; Acharya, S. Large eddy simulations of flow and heat transfer in rotating ribbed duct flows. *J. Heat Transf.* **2005**, *127*, 486–498. [[CrossRef](#)]
51. Saha, A.K.; Acharya, S. Flow and heat transfer in an internally ribbed duct with rotation: An assessment of large eddy simulations and unsteady Reynolds-averaged Navier-Stokes simulations. *J. Turbomach.* **2005**, *127*, 306–320. [[CrossRef](#)]
52. Saha, A.; Acharya, S. Turbulent heat transfer in ribbed coolant passages of different aspect ratios: Parametric effects. *J. Heat Transf.* **2007**, *129*, 449–463. [[CrossRef](#)]
53. Liu, Y.; Tucker, P.G.; Iacono, G.L. Comparison of zonal RANS and LES for a non-isothermal ribbed channel flow. *Int. J. Heat Fluid Flow* **2006**, *27*, 391–401. [[CrossRef](#)]
54. Tyacke, J.; Tucker, P.G. Large eddy simulation of turbine internal cooling ducts. *Comput. Fluids* **2015**, *114*, 130–140. [[CrossRef](#)]
55. Tyacke, J.C.; Dai, Y.; Tucker, P.G. Impact of rib shape on heat transfer using LES. *Appl. Math. Model.* **2021**, *97*, 244–267. [[CrossRef](#)]
56. Lohász, M.M.; Rambaud, P.; Benocci, C. Flow features in a fully developed ribbed duct flow as a result of MILES. *Flow Turbul. Combust.* **2006**, *77*, 59–76. [[CrossRef](#)]
57. Scholl, S.; Verstraete, T.; Torres-Garcia, J.; Duchaine, F.; Gicquel, L.Y.M. Influence of the thermal boundary conditions on the heat transfer of a rib-roughened cooling channel using LES. *Proc. Inst. Mech. Eng. A* **2015**, *229*, 498–507. [[CrossRef](#)]
58. Scholl, S.; Verstraete, T.; Duchaine, F.; Gicquel, L. Conjugate heat transfer of a rib-roughened internal turbine blade cooling channel using large eddy simulation. *Int. J. Heat Fluid Flow* **2016**, *61*, 650–664. [[CrossRef](#)]
59. Ramgadia, A.G.; Saha, A.K. Large eddy simulation of turbulent flow and heat transfer in a ribbed coolant passage. *J. Appl. Math.* **2012**, *2012*, 246313. [[CrossRef](#)]
60. Borello, D.; Salvagni, A.; Hanjalić, K. Effects of rotation on flow in an asymmetric rib-roughened duct: LES study. *Int. J. Heat Fluid Flow* **2015**, *55*, 104–119. [[CrossRef](#)]
61. Salvagni, A.; Borello, D.; Rispoli, F.; Hanjalić, K. Large-eddy simulations of heat transfer in asymmetric rib-roughened ducts: Effects of rotation. *Int. J. Heat Fluid Flow* **2017**, *68*, 373–385. [[CrossRef](#)]
62. Labbé, O. Large-eddy-simulation of flow and heat transfer in a ribbed duct. *Comput. Fluids* **2013**, *76*, 23–32. [[CrossRef](#)]
63. Jiang, Z.; Xiao, Z.; Shi, Y.; Chen, S. Constrained large-eddy simulation of turbulent flow and heat transfer in a stationary ribbed duct. *Int. J. Numer. Methods Heat Fluid Flow* **2016**, *26*, 1069–1091. [[CrossRef](#)]
64. Fang, X.; Yang, Z.; Wang, B.C.; Tachie, M.F.; Bergstrom, D.J. Highly-disturbed turbulent flow in a square channel with V-shaped ribs on one wall. *Int. J. Heat Fluid Flow* **2015**, *56*, 182–197. [[CrossRef](#)]
65. Fang, X.; Yang, Z.; Wang, B.C.; Tachie, M.F.; Bergstrom, D.J. Large-eddy simulation of turbulent flow and structures in a square duct roughened with perpendicular and V-shaped ribs. *Phys. Fluids* **2017**, *29*, 065110. [[CrossRef](#)]
66. Mahmoodi-Jezeh, S.V.; Wang, B.C. Direct numerical simulation of turbulent heat transfer in a square duct with transverse ribs mounted on one wall. *Int. J. Heat Fluid Flow* **2021**, *89*, 108782. [[CrossRef](#)]
67. Matsubara, K.; Ohta, H.; Miura, T. Entrance region heat transfer in a channel with a ribbed wall. *J. Heat Transf.* **2016**, *138*, 122001. [[CrossRef](#)]
68. Matsubara, K.; Ohta, H.; Ishino, T. Direct simulation of inlet region heat transfer in a channel with repeated ribs under iso-thermal wall heating condition. *Int. J. Therm. Sci.* **2020**, *154*, 106408. [[CrossRef](#)]
69. Song, J.C.; Ahn, J.; Lee, J.S. An immersed-boundary method for conjugate heat transfer analysis. *J. Mech. Sci. Technol.* **2017**, *31*, 2287–2294. [[CrossRef](#)]
70. Ahn, J.; Song, J.C.; Lee, J.S. Dependence of conjugate heat transfer in ribbed channel on thermal conductivity of channel wall: An LES study. *Energies* **2021**, *14*, 5698. [[CrossRef](#)]
71. Ahn, J.; Song, J.C.; Lee, J.S. Large eddy simulation of conjugate heat transfer in a ribbed channel: Reynolds number effect. *Processes* **2022**, *10*, 1928. [[CrossRef](#)]
72. Abdelmoula, A.; Younis, B.A.; Spring, S.; Weigand, B. Large-eddy simulations of heated flows in ribbed channels with spanwise rotation. *Numer. Heat Transf. A* **2018**, *74*, 895–916. [[CrossRef](#)]
73. Ruck, S.; Arbeiter, F. Detached eddy simulation of turbulent flow and heat transfer in cooling channels roughened by variously shaped ribs on one wall. *Int. J. Heat Mass Transf.* **2018**, *118*, 388–401. [[CrossRef](#)]

74. Duchaine, F.; Gicquel, L.; Grosnickel, T.; Koupper, C. Large-eddy simulation of the flow developing in static and rotating ribbed channels. *J. Turbomach.* **2020**, *142*, 041003. [[CrossRef](#)]
75. Perrot, A.; Gicquel, L.; Duchaine, F.; Odier, N.; Dombard, J.; Grosnickel, T. Unsteady analysis of heat transfer coefficient distribution in a static ribbed channel for an established flow. *J. Turbomach.* **2021**, *143*, 121004. [[CrossRef](#)]
76. Zhiyin, Y. Large-eddy simulation: Past, present and the future. *Chin. J. Aeronaut.* **2015**, *28*, 11–24. [[CrossRef](#)]
77. Oliver, T.A.; Bogard, D.G.; Moser, R.D. Large eddy simulation of compressible, shaped-hole film cooling. *Int. J. Heat Mass Transf.* **2019**, *140*, 498–517. [[CrossRef](#)]
78. Ahn, J. Large eddy simulation of film cooling: A review. *Energies* **2022**, *15*, 8876. [[CrossRef](#)]
79. Patankar, S.V.; Liu, C.H.; Sparrow, E.M. Fully developed flow and heat transfer in ducts having streamwise-periodic variations of cross-sectional area. *J. Heat Transf.* **1977**, *99*, 180–186. [[CrossRef](#)]
80. Germano, M.; Piomelli, P.; Moin, P.; Cabot, W.H. A dynamic sub-grid scale eddy viscosity model. *Phys. Fluids* **1991**, *A3*, 1760–1765. [[CrossRef](#)]
81. Anderson, R.; Meneveau, C. Effects of the similarity model in finite-difference LES of isotropic turbulence using a Lagrangian dynamic mixed model. *Flow Turbul. Combust.* **1999**, *62*, 201–225. [[CrossRef](#)]
82. Stoll, R.; Porté-Agel, F. Large-eddy simulation of the stable atmospheric boundary layer using dynamic models with different averaging schemes. *Bound. Layer Meteorol.* **2008**, *126*, 1–28. [[CrossRef](#)]
83. Ooi, A.; Iaccarino, G.; Durbin, P.A.; Behnia, M. Reynolds averaged simulation of flow and heat transfer in ribbed ducts. *Int. J. Heat Fluid Flow* **2002**, *23*, 750–757. [[CrossRef](#)]
84. Rau, G.; Çakan, M.; Moeller, D.; Arts, T. The effect of periodic ribs on the local aerodynamic and heat transfer performance of a straight cooling channel. *J. Turbomach.* **1998**, *120*, 368–375. [[CrossRef](#)]
85. Cho, H.H.; Wu, S.J.; Kwon, H.J. Local heat/mass transfer measurements in a rectangular duct with discrete ribs. *J. Turbomach.* **2000**, *122*, 579–586. [[CrossRef](#)]
86. Liou, T.M.; Hwang, J.J. Effect of ridge shapes on turbulent heat transfer and friction in a rectangular channel. *Int. J. Heat Mass Transf.* **1993**, *36*, 931–940. [[CrossRef](#)]
87. Cukurel, B.; Arts, T. Local heat transfer dependency on thermal boundary condition in ribbed cooling channel geometries. *J. Heat Transfer* **2013**, *135*, 101001. [[CrossRef](#)]
88. Iaccarino, G.; Ooi, A.; Durbin, P.A.; Behnia, M. Conjugate heat transfer predictions in two-dimensional ribbed passages. *Int. J. Heat Fluid Flow* **2002**, *23*, 340–345. [[CrossRef](#)]
89. Cukurel, B.; Arts, T.; Selcan, C. Conjugate heat transfer characterization in cooling channels. *J. Therm. Sci.* **2012**, *21*, 286–294. [[CrossRef](#)]
90. Jung, E.Y.; Chung, H.; Choi, S.M.; Woo, T.-K.; Cho, H.H. Conjugate heat transfer on full-coverage film cooling with array jet impingement with various Biot numbers. *Exp. Thermal Fluid Sci.* **2017**, *83*, 1–8. [[CrossRef](#)]
91. Kim, K.M.; Kim, Y.Y.; Lee, D.H.; Rhee, D.H.; Cho, H.H. Influence of duct aspect ratio on heat/mass transfer in coolant passages with rotation. *Int. J. Heat Fluid Flow* **2007**, *28*, 357–373. [[CrossRef](#)]
92. Schüler, M.; Zehnder, F.; Weigand, B.; von Wolfersdorf, J.; Neumann, S.O. The effect of turning vanes on pressure loss and heat transfer of a ribbed rectangular two-pass internal cooling channel. *J. Turbomach.* **2011**, *133*, 021017. [[CrossRef](#)]
93. Krishnaswamy, K.; Sivan, S. Improvement in thermal hydraulic performance by using continuous V and W-shaped rib turbulators in gas turbine blade cooling application. *Case Stud. Therm. Eng.* **2021**, *24*, 100857. [[CrossRef](#)]
94. Ahn, J.; Kim, M.S.; Jang, S. Effects of cross-sectional aspect ratio of V-shaped ribs and blockage ratio on heat transfer in a channel at a low Reynolds number. *J. Mech. Sci. Technol.* **2018**, *32*, 5465–5473. [[CrossRef](#)]
95. Lee, D.H.; Rhee, D.H.; Kim, K.M.; Cho, H.H.; Moon, H.K. Detailed measurement of heat/mass transfer with continuous and multiple V-shaped ribs in rectangular channel. *Energy* **2009**, *24*, 1770–1778. [[CrossRef](#)]
96. Jin, D.; Zuo, J.; Quan, S.; Xu, S.; Gao, H. Thermohydraulic performance of solar air heater with staggered multiple V-shaped ribs on the absorber plate. *Energy* **2017**, *127*, 68–77. [[CrossRef](#)]
97. Moon, M.A.; Park, M.J.; Kim, K.Y. Evaluation of heat transfer performances of various rib shapes. *Int. J. Heat Mass Transf.* **2014**, *71*, 275–284. [[CrossRef](#)]
98. Togun, H.; Hamidatou, S.; Mohammed, H.I.; Abed, A.M.; Hasan, H.A.; Homod, R.Z.; Al-Fatlawi, A.W.; Al-Thamir, M.; Abdulrazzaq, T. Numerical Simulation on Heat Transfer Augmentation by Using Innovative Hybrid Ribs in a Forward-Facing Contracting Channel. *Symmetry* **2023**, *15*, 690. [[CrossRef](#)]
99. Liou, T.; Wang, W.; Chang, Y. Holographic interferometry study of spatially periodic heat transfer in a channel with ribs detached from one wall. *J. Heat Transfer* **1995**, *117*, 32–39. [[CrossRef](#)]
100. Kim, S.; Suh, S.; Baek, S.; Hwang, W. The effect of single-sided ribs on heat transfer and pressure drop within a trailing edge internal channel of a gas turbine blade. *J. Thermal Sci. Eng. Appl.* **2022**, *14*, 081005. [[CrossRef](#)]
101. Elyyan, M.A.; Tafti, D.K. Large eddy simulation investigation of flow and heat transfer in a channel with dimples and protrusions. *J. Turbomach.* **2008**, *130*, 041016. [[CrossRef](#)]
102. Lee, Y.O.; Ahn, J.; Kim, J.; Lee, J.S. Effect of dimple arrangements on the turbulent heat transfer in a dimpled channel. *J. Enhanced Heat Transf.* **2012**, *19*, 359–367. [[CrossRef](#)]

103. Hao, Z.; Górlé, C. Large eddy simulations of forced heat convection in a pin-fin array with a priori examination of an eddy-viscosity turbulence model. *Int. J. Heat Fluid Flow* **2019**, *77*, 73–83. [[CrossRef](#)]
104. Fan, X.; Li, L.; Zou, J.; Zhou, Y. Cooling methods for gas turbine blade leading edge: Comparative study on impingement cooling, vortex cooling and double vortex cooling. *Int. Commun. Heat Mass Transf.* **2019**, *100*, 133–145. [[CrossRef](#)]

Disclaimer/Publisher’s Note: The statements, opinions and data contained in all publications are solely those of the individual author(s) and contributor(s) and not of MDPI and/or the editor(s). MDPI and/or the editor(s) disclaim responsibility for any injury to people or property resulting from any ideas, methods, instructions or products referred to in the content.